Journal of Biomechanics 47 (2014) 639–644

Contents lists available at ScienceDirect

Journal of Biomechanics

journal homepage: www.elsevier.com/locate/jbiomech
www.JBiomech.com

High-resolution mechanical imaging of the kidney

Kaspar-Josche Streitberger [a], Jing Guo [a], Heiko Tzschätzsch [a], Sebastian Hirsch [a], Thomas Fischer [a], Jürgen Braun [b], Ingolf Sack [a,*]

[a] Department of Radiology, Charité – Universitätsmedizin Berlin, Campus Charité Mitte, Berlin, Germany
[b] Institute of Medical Informatics, Charité – Universitätsmedizin Berlin, Campus Benjamin Franklin, Berlin, Germany

ARTICLE INFO

Article history:
Accepted 27 November 2013

Keywords:
Kidney
Viscoelasticity
Time harmonic elastography
Shear modulus
Pressure
3D multifrequency MRE
Multifrequency inversion

ABSTRACT

The objective of this study was to test the feasibility and reproducibility of *in vivo* high-resolution mechanical imaging of the asymptomatic human kidney. Hereby nine volunteers were examined at three different physiological states of urinary bladder filling (a normal state, urinary urgency, and immediately after urinary relief). Mechanical imaging was performed of the *in vivo* kidney using three-dimensional multifrequency magnetic resonance elastography combined with multifrequency dual elastovisco inversion. Other than in classical elastography, where the storage and loss shear moduli are evaluated, we analyzed the magnitude $|G^*|$ and the phase angle φ of the complex shear modulus reconstructed by simultaneous inversion of full wave field data corresponding to 7 harmonic drive frequencies from 30 to 60 Hz and a resolution of 2.5 mm cubic voxel size.

Mechanical parameter maps were derived with a spatial resolution superior to that in previous work. The group-averaged values of $|G^*|$ were 2.67 ± 0.52 kPa in the renal medulla, 1.64 ± 0.17 kPa in the cortex, and 1.17 ± 0.21 kPa in the hilus. The phase angle φ (in radians) was 0.89 ± 0.12 in the medulla, 0.83 ± 0.09 in the cortex, and 0.72 ± 0.06 in the hilus. All regional differences were significant ($P < 0.001$), while no significant variation was found in relation to different stages of bladder filling.

In summary our study provides first high-resolution maps of viscoelastic parameters of the three anatomical regions of the kidney. $|G^*|$ and φ provide novel information on the viscoelastic properties of the kidney, which is potentially useful for the detection of renal lesions or fibrosis.

1. Introduction

Proper renal function is essential for whole body homeostasis such as the excretion of nitrogenous byproducts, the regulation of electrolytes and extracellular fluid volume, as well as the maintenance of the body's acid–base balance. With their endocrine function the kidneys also coordinate long-term blood pressure regulation. End-stage renal failure is associated with conditions such as serious electrolyte imbalance or increased acid levels and anemia, and affected patients may require long-term hemodialysis or a kidney transplant (Wolfe et al., 1999). The incidence and prevalence of diabetes and hypertension-associated chronic kidney disease (CKD) are on the rise (El Nahas, 2005; Coresh et al., 2007).

CKD such as glomerulonephritis, obstructive nephropathy, interstitial nephritis, and cystic nephropathies are invariably accompanied by renal fibrosis as a result of an excessive accumulation of extracellular matrix through the activation of fibroblasts and myofibroblasts (Cho, 2010; Wynn, 2008).

The noninvasive detection and quantification of these fibrotic changes, especially in early stages, by the altered mechanical properties of the kidney could be beneficial for the diagnosis and monitoring the response to treatment. So far, in vivo ultrasound elastography has been successfully used in allograft kidney transplants (Arndt et al., 2010; Sommerer et al., 2013). A correlation between the grade of fibrosis and renal stiffness parameters as shown by Arndt et al. (2010) and Sommerer et al. (2013) was not observed by Grenier et al. (2012) and remains a matter of debate. The penetration depth of ultrasound-based elastography, however, is restricted due to the high absorption rates of both ultrasound signal and transient shear waves (Sandrin et al., 2003), limiting the accessibility of the *in vivo* kidney, especially in obese patients.

These restrictions only partially apply to magnetic resonance elastography (MRE) (Muthupillai and Ehman, 1996) where the maximum diagnostic depth is less constrained due to the lower damping rate of continuously excited time–harmonic shear waves at very low frequencies between 25 Hz and 60 Hz. MRE has been proven sensitive to hepatic fibrosis and is increasingly integrated into diagnostic liver examinations in the routine clinical setting

* Correspondence to: Department of Radiology, Charité - Universitätsmedizin Berlin, Charitéplatz 1, 10117 Berlin, Germany. Tel.: +49 30 450 539 058; fax: +49 30 450 539 988.
E-mail address: ingolf.sack@charite.de (I. Sack).

0021-9290/$ - see front matter © 2013 Elsevier Ltd. All rights reserved.
http://dx.doi.org/10.1016/j.jbiomech.2013.11.051

(Venkatesh et al., 2013; Lee et al., 2013). Previous MRE studies on human and animal kidneys have shown regional differences in viscoelastic properties (Bensamoun et al., 2011; Rouviere et al., 2011; Warner et al., 2011; Korsmo et al., 2013). However, mechanical parameter maps of the kidney have been limited by low spatial resolution, rendering a clear distinction between cortex, medulla, and hilus difficult.

To improve the spatial resolution in MRE, the grid of voxels that encodes the externally induced shear waves should be refined. Additionally, the computation of tissue mechanical parameters from shear waves needs to be revised, since the solution of the inverse problem in elastography is ill-posed and thus remains an obstacle to high-resolution MRE. A recent approach that addresses resolution improvements in wave images and elastograms of the liver and the spleen combines fast echo-planar-imaging (EPI) with 3D multifrequency wave field acquisition (3DMMRE) (Hirsch et al., 2013; Guo et al., 2013). With this technique, 3D dynamic wave fields are invoked by multifrequency dual elastovisco (MDEV) inversion for calculating the magnitude and the phase angle of the complex-valued shear modulus, G^* (Papazoglou et al., 2012). MDEV inversion is capable of compensating for destructive interferences regularly arising in single-frequency wave patterns.

We here adopt this technique to generate viscoelastic maps of the asymptomatic human kidney that clearly delinate the three anatomical regions of the kidney – the cortex, the medulla, and the hilus. Furthermore, we test the influence of three physiological conditions characterized by a normal (nonspecific, relaxed) state, a full-bladder state, and a state of emptied bladder in nine healthy volunteers.

The acquired data are intended as a reference for potential diagnostic applications of high-resolution mechanical imaging of the *in vivo* kidney.

2. Methods

The study was approved by the local institutional review board. Nine healthy volunteers (1 woman; mean age 34 ± 8.8 years) were included in this study. Each volunteer was examined three times on two different days: day 1 without specific consideration of urinary bladder filling; day 2, twice in consecutive experiments with full and empty bladder. In addition to MRE, a clinical protocol including T1-, T2- and proton-density-weighted anatomical sequences were used for three-dimensional kidney imaging. Imaging slices for MRE were positioned in transverse orientation within the region of greatest overlap of both kidneys.

2.1. DMMRE

Vibrations were generated by a customized nonmagnetic driver, which was mounted at the end of the patient table (Hirsch et al., 2013). A carbon fiber rod was used to transfer the vibrations to a rubber mat placed over the umbilical and lumbar regions (transtubercular plane) of the volunteers. The transducer mat was fixed using a commercially obtainable kidney belt and velcro strips (Fig. 1).

The experiments were run on a 1.5-Tesla MRI scanner (Magnetom Sonata; Siemens Erlangen, Germany) using a 12-channel body surface coil. For rapid motion field acquisition, a 2D single-shot spin-echo echo-planar imaging (EPI) sequence with a trapezoidal flow-compensated motion-encoding gradient (MEG), consecutively applied along all three axes of the scanner coordinate system, was used. To allow the mechanical waves to propagate into the tissue, the vibration was initiated through a trigger pulse by the scanner at least 100 ms before the start of the MEG. The vibration frequencies used in this experiment were 30, 35, 40, 45, 50, 55, and 60 Hz. The trigger pulse was delayed in consecutive time-resolved scans by increments of $1/8 \times f$ (vibration frequency f), yielding 8 dynamics of a wave cycles. For 10 adjacent slices of $2.5 \times 2.5 \times 2.5$ mm^3 resolution (voxel volume 15.625 mm^3), 7 frequencies, 8 wave dynamics, and 3 MEG directions, a total of 1680 images were averaged twice to increase the signal-to-noise ratio (SNR). Further imaging parameters were, repetition time (TR) 1770 ms, echo time (TE) 55 ms, field of view (FoV) 260×260 mm^2, matrix size 104×104, parallel imaging with a GRAPPA factor of 2, MEG frequency 50.6 Hz (to fit one MEG cycle into TE/2, implying the principle of fractional motion encoding (Rump et al., 2007), MEG amplitude 30 mT/m, 1.4 min scan time for each frequency, resulting in a total acquisition time of under 10 min for one 3DMMRE examination.

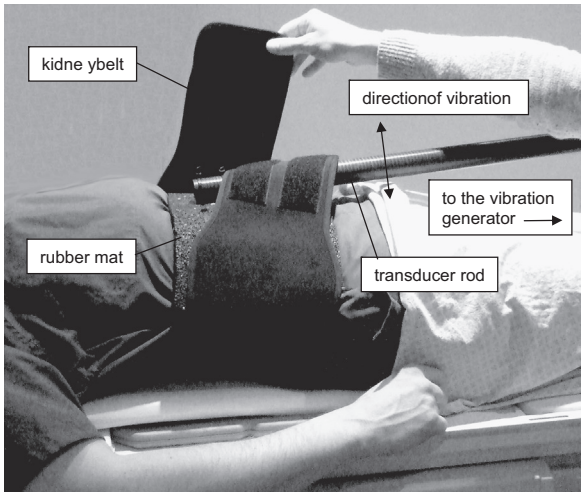

Fig. 1. Experimental setup for mechanical stimulation of the kidney showing the transducer mat, which was positioned and fixed using a commercially obtainable kidney belt and velcro strips. The transducer rod was mounted to a nonmagnetic driver as shown in (Hirsch et al., 2013).

2.2. Data processing

Postprocessing was performed as previously described in (Hirsch et al., 2013). Briefly, the following postprocessing steps were applied: (1) phase unwrapping based on spatial gradients (Papazoglou et al., 2009). The numerical derivatives were calculated by 3D gradients according to (Anderssen and Hegland, 1999) using the averaging scheme with a cubic 3D kernel of five pixel edge length; (2) calculation of the curl components by the resulting strain components from step 1 for suppression of volumetric strain (Sinkus et al., 2005) (3) temporal Fourier transformation and selection of the complex curl field for each drive frequency; (4) noise suppression by a weak Butterworth low-pass filter with $k = 100\ \mathrm{m}^{-1}$ threshold; (5) for each slice, a total of 21 complex-valued wave images (3 curl components and 7 frequencies) were combined by MDEV inversion for the reconstruction of the magnitude of the complex shear modulus $|G^*|$ and its loss angle φ in two separated inversion steps yielding 2×10 parameter maps. An example of the complex-valued curl-field in a central image slice of one volunteer is shown in Fig. 2 by the third curl-component at seven frequencies. Additionally, the amount of induced shear strain is illustrated by the scalar octahedral shear strain as proposed by as a measure of shear deflection amplitude in MRE (McGarry et al., 2011).

2.3. Statistical analysis

The results are tabulated as arithmetic mean $\pm$ standard deviation. The influence of bladder filling on the viscoelastic properties $|G^*|$ and φ as well as intrarenal regional differences in $|G^*|$ and φ was analyzed by two-tailed paired Student's t-test and a repeated-measurement ANOVA for testing the effect of physiological bladder states. A P-value < 0.05 was considered statistically significant. All calculations were performed using the MATLAB Statistics Toolbox (MathWorks, Natick, Massachusetts, USA).

3. Results

The examinations were well tolerated by all nine healthy volunteers at all stages of bladder filling. The position of each volunteer on the MRI patient table was marked to achieve reproducible slice positioning.

MDEV parameter maps of one volunteer are shown in Fig. 3. Spatial averaging was performed according to the manually segmented anatomical regions of the kidney – the cortex, the medulla, and the hilus – as outlined in the MRE magnitude images. Additionally, spatial averaging was performed according to a separately segmented region comprising the whole renal parenchyma visible in the image slices. The mean stiffness of the whole kidney was $|G^*| = 1.83 \pm 0.25$ kPa and the phase angle φ was 0.82 ± 0.08. Significant regional differences were observed in both $|G^*|$ and φ as shown in Fig. 4. The mean stiffness of the medullary